Proceedings of SPIE, Vol. 4742, April 2002

Ultrasonic Displacement Sensor for the Seismic Detection of Buried Land Mines

James S. Martin[a], Douglas J. Fenneman[a], Fabien Codron[a], Peter H. Rogers[a], Waymond R. Scott, Jr. [b], Gregg D. Larson [a], and George S. McCall II [c]
[a] School of Mechanical Engineering
[b] School of Electrical and Computer Engineering
[c] Georgia Tech Research Institute
Georgia Institute of Technology
Atlanta, GA 30332

ABSTRACT

A system is under development that uses seismic surface waves to detect and image buried landmines. The system, which has been previously reported in the literature, requires a sensor that does not contact the soil surface. Thus, the seismic signal can be evaluated directly above a candidate mine location. The system can then utilize small amplitude and non-propagating components of the seismic wave field to form an image. Currently, a radar-based sensor is being used in this system. A less expensive alternative to this is an ultrasonic sensor that works on similar principles to the radar but exploits a much slower acoustic wave speed to achieve comparable performance at an operating frequency 5 to 6 decades below the radar frequency. The prototype ultrasonic sensor interrogates the soil with a 50 kHz acoustic signal. This signal is reflected from the soil surface and phase modulated by the surface motion. The displacement can be extracted from this modulation using either analog or digital electronics. The analog scheme appears to offer both the lowest cost and the best performance in initial testing. The sensor has been tested using damp compacted sand as a soil surrogate and has demonstrated a spatial resolution and signal-to-noise ratio comparable to those that have been achieved with the radar sensor. In addition to being low-cost, the ultrasonic sensor also offers the potential advantage of penetrating different forms of ground cover than those that are permeable to the radar signal. This is because density and stiffness contrasts mediate ultrasonic reflections whereas electromagnetic reflection is governed by dielectric contrast.

Keywords: land mine, mine detection, ultrasound, seismic waves

1. INTRODUCTION

Work has been going on at Georgia Tech for several years on the development of a landmine detection scheme which employs audio frequency seismic surface waves (Rayleigh waves) to detect and image buried land mines[1,2]. The basic concept of this scheme is that an array of non-contacting vibrometers can be used to image the seismic wave field over an entire region of interest, including directly above a buried mine. In this way a substantial amount of spatial and temporal information is available from which to form an image. Also, many of the signal-to-noise and signal-to-reverberation problems that would arise in a pulse-echo seismic detection scheme can be avoided by eliminating the need for the seismic echo to propagate to a remote receiver location[3]. The prototype system, which has been constructed to test this concept, is depicted in figure 1. Here the receiving array is synthesized using a single sensor and an automatic positioning system. This substantially simplifies the experimental problem but is not practical for a field operable system because of the long scan times required to synthesize the array. The sensor employed in the prototype system is a radar-based design that illuminates the ground with a continuous 8 GHz signal and deduces the surface vibration from the modulation of the reflected radar signal. Both the sensor and the prototype system have shown great promise for the reliable detection of all types of buried mines, particularly low-metal anti-personnel mines, in initial testing. The reason for this is that mines have mechanical properties that are significantly different from soils and typical forms of clutter. Their interactions with seismic waves are therefore unique and provide an excellent detection cue.

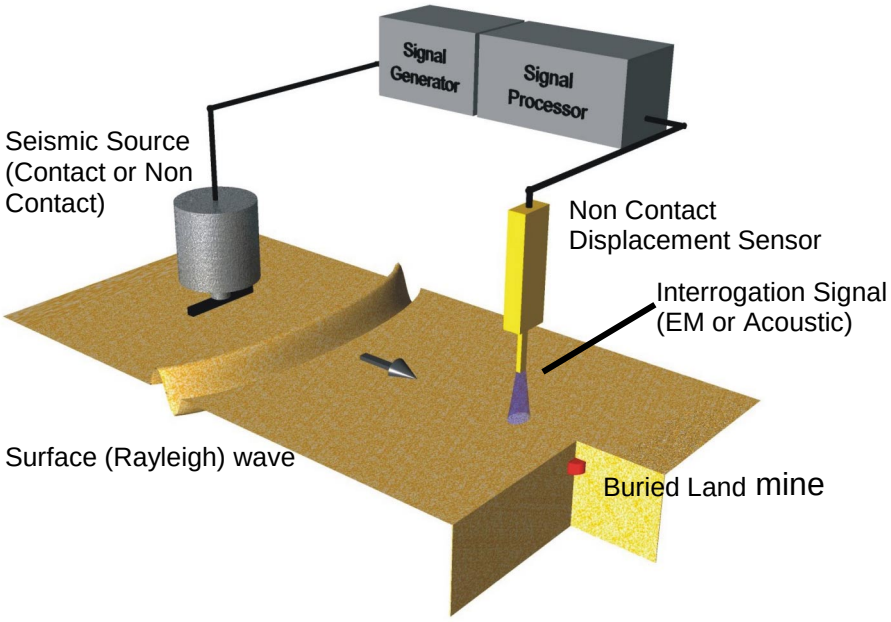

Figure 1: Seismic Mine Detection System

The operating frequency of the radar sensor was driven by a compromise between competing wavelength requirements. Some of these, such as penetrating surface cover, insensitivity to surface roughness, and fast scanning speed, favor long wavelengths. Others, such as sensitivity to small displacements and fine spatial resolution (small spot size), favor short wavelengths. By selecting an acoustic rather than an electromagnetic signal to interrogate the soil surface, it is possible to achieve a similar wavelength with a much lower operating frequency because of the nearly 10^6 ratio of these two wave speeds in air. This lower operating frequency offers several possible advantages. Foremost among these is the cost savings associated with the transducers and analog components required for the operation of an ultrasonic sensor as compared with a radar sensor. This is an important consideration in the construction of physical arrays, which could easily involve hundreds of sensors. A direct cost comparison between the two sensors is difficult because the ultrasonic sensor has not yet reached a state of development and testing comparable to the radar sensor's. However, comparison with a similarly capable radar sensor (one without a focussing antenna) suggests that the cost savings may be a factor of ten with the ultrasonic sensor requiring less than $1,000 worth of components, all of which can be purchased from vendor stock.

2. PRINCIPLES OF SENSOR OPERATION

Both the ultrasonic sensor and the radar sensor operate on similar principles. Each sensor deduces the nearly instantaneous surface displacement from phase modulation of a reflected signal. The operations involved may be represented as follows [4]: A high frequency pure tone signal of the form $A_1\cos(\omega_h t)$ is transmitted to, and reflected from, the soil surface. When the signal is received it contains a phase term due to the transit time between the transmitter and receiver. This term has both a constant phase component (D) due to the total path length and a time-dependant component ($\delta(t)$) due to changes in the path length caused by the displacement of the vibrating surface that is the source of the reflection. The received signal will then have the form:

$$rec = A_2 \cos\left(\omega_h t + k_h \left(D + \delta(t)\right)\right) \qquad (1)$$

where k_h is the wavenumber of the high frequency signal ($k_h=\omega_h/c$), and c is the propagation speed which may be that of either light or sound depending on the nature of the interrogation signal. The amplitude coefficient A_2 accounts for the reflectivity of the vibrating surface, propagation loss, and transducer sensitivity. If the received

signal is multiplied with the original carrier signal the result can be expanded into the sum of two cosines containing the sum and difference of the arguments of the contributing functions as follows:

$$mix_1 = A_1 A_2 \left[\tfrac{1}{2}\cos\left(-k_h\left(D+\delta(t)\right)\right)+\cos\left(2\omega_h t + k_h\left(D+\delta(t)\right)\right)\right] \qquad (2)$$

The second term in equation 2 has a time dependence on the order of twice the carrier frequency, whereas the first term contains the much lower frequency content of the function δ(t) that represents the surface vibration. Separation of the first term from this equation can, therefore, be easily achieved with a low-pass filter. The first term may be expanded as a sum of cosine-sine products. If the wavelength of the high frequency signal is assumed to be much longer than the peak amplitude of the time varying path length change (δ(t)), then the product $k_h\delta(t)$ will be much less than unity. Here the sine of this product may be approximated by the argument and the cosine of this product with unity. Thus, the low frequency component of equation 2 contains two terms:

$$LF_1 = \tfrac{1}{2} A_1 A_2 \cos(k_h D) - \tfrac{1}{2} A_1 A_2 k_h \sin(k_h D)\delta(t) \qquad (3)$$

Here the first term is time-independent and the second term is directly proportional to the time-dependent path length change with a proportionality constant that depends on both the total path length and the magnitude of the received signal. Since neither of these factors may be known a priori, it is necessary to perform an additional multiplication in order to extract δ(t). This is a multiplication of the received signal with a signal that is in quadrature with the original transmitted signal (i.e. of the form: $A_1\sin(\omega_h t)$). The multiplication is carried out similar to the first and yields a low frequency term with the sine and cosine functions reversed from those in expression 3. This result has the form:

$$LF_2 = -\tfrac{1}{2} A_1 A_2 \sin(k_h D) - \tfrac{1}{2} A_1 A_2 k_h \cos(k_h D)\delta(t) \qquad (4)$$

Expressions 3 and 4 represent the low frequency results of two mixing operations that may be arbitrarily defined as mix 1 and mix 2. The time-independent and time-dependent components of these expressions may be separated using high-pass and low-pass filters set well below the lowest spectral components of the time varying path length. This spectrum is known a priori since the low frequency motion is produced artificially. The results of these filtering operations can then be combined to form the expression:

$$\delta(t) = \left(\frac{1}{k_h}\right)\frac{\left(DC_{mix1}\right)\cdot\left(AC_{mix2}\right)+\left(DC_{mix2}\right)\cdot\left(AC_{mix1}\right)}{\left(DC_{mix1}\right)^2+\left(DC_{mix2}\right)^2} \qquad (5)$$

In equation 5, DC and AC indicate the low-passed and high-passed signals extracted from the LF_1 and LF_2 respectively. The right side of equation 5 is entirely known from the measurement and filtering operations and from the medium (i.e. the wave speed) in which the carrier signal propagates.

In a surface-normal monostatic non-contact sensor, the path length variation is twice the surface displacement since surface motion acts to shorten or lengthen both the incoming and the reflected path. In a bistatic non-contact sensor, an additional factor of the sine of the half angle at which the transmitting and reflecting beams intersect relates these quantities. For the ultrasound sensor, which was operated in bistatic mode, the half angle was 30° so the path length variation was equal to the surface displacement. This can be seen graphically in figure 2. Here it is important to note that the picture is, by necessity, out of scale. The actual acoustic path length is greater by a factor of at least 10^5 than the surface displacement, and therefore the angular deflection of the beam (α) may be neglected. The bistatic configuration constituted a 6-dB loss in sensitivity relative to the monostatic mode, which was employed for the radar sensor, but offered other benefits that will be discussed later.

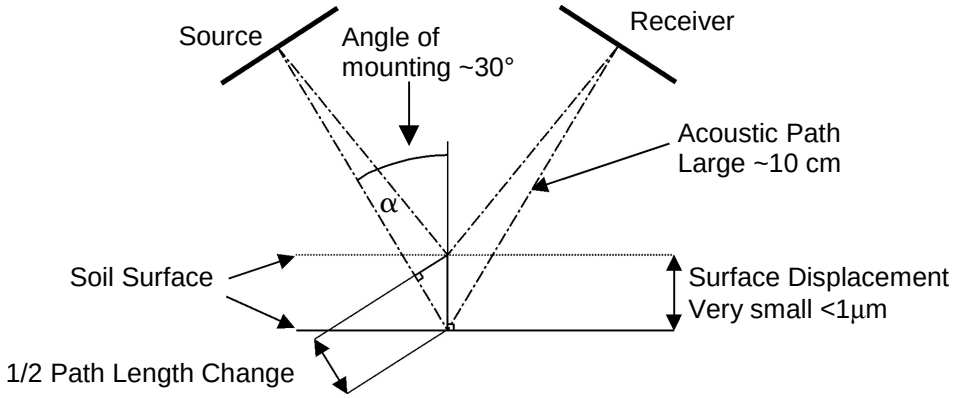

Figure 2: Bistatic Geometry of Ultrasonic Vibrometer

3. DEMODULATION SCHEMES

In practice, the demodulation scheme described in equation 5 may be implemented in many ways. Each of the required multiplications, filtering operations, or summations can be performed either in analog electronics or digitally. For the radar sensor, only the final operation involving low frequency terms is performed digitally. The initial multiplication and operations involving its unfiltered products would require a digitizer operating well in excess of the 8 GHz carrier frequency. The first multiplication and low pass filtering operation are, therefore carried out with passive mixers and filters. The much lower operating frequencies of the ultrasound sensor prompted a reconsideration of this arrangement. Low-cost digitizers that operate above 100 kHz are readily available. In fact, the digitizer used to sample the low frequency components of the mixer outputs of the radar sensor could adequately sample the 50 kHz carrier signal chosen for the ultrasound sensor simultaneously on up to 12 channels. A fully digital demodulation scheme was therefore considered for the ultrasound sensor.

Two potential pitfalls arise in a fully digital demodulation scheme. These are the limits imposed by the bit resolution and by the clock stability of the digitizer. In practice, these would act in concert to increase the apparent broadband noise floor on the acquired carrier signal. For simplicity in evaluating the requirements of the system, each effect was considered separately. Figure 3 shows the results of sampling a 50 kHz carrier signal with side lobes at ± 200 Hz using both a 12-bit and a 16-bit coding scheme using 1-Hz frequency resolution. The side lobes are 100 dB below the carrier, which is at the limit of the dynamic range of the coding. This represents the effect of modulating the carrier by reflection from a surface vibrating continuously at 200 Hz with an amplitude of vibration of 10 nm following the equations presented by Cox and Rogers [5,6] for a similar system operating under water. It can be seen from figure 3 that the noise floor imposed by the 12 bit coding is nearly 20 dB below the side lobes. This corresponds to an apparent displacement of slightly more than 1 nm, which is close to the resolution achieved with the radar sensor. With 16 bit coding there is a 20-dB improvement beyond this performance. The apparent noise introduced by jitter in the digitizer clock is a more difficult thing to quantify. Manufacturer's specifications were found to be inadequate in this regard, and the clock stability was instead determined experimentally for the available digitizer, which was a National Instruments PCI-MIO-16E1 12 bit 1.2 MHz card inside a Pentium III personal computer. There was some uncertainty in this measurement in that no attempt was made to distinguish between sources of clock noise innate to the card and noise introduced by the PC. Figure 4 depicts spectra similar to those in figure 3 where the time samples are represented with 32 bit integers and shifted randomly by the 50-nS jitter inferred for the existing digitizer and by a 5-nS jitter presumed for a superior card. It can be seen from the figure that even the superior card is unable to achieve the performance limitations of 12 bit coding and this, in turn, was barely sufficient to match the sensitivity of the radar sensor. It is possible that a more sophisticated card and a combination of over sampling and averaging might improve performance to an acceptable level. However, given the cost per channel, the uncertain potential of a new digitizer, and the obvious dynamic range limitations inherent in bit coding the signal, the fully digital demodulation scheme was rejected.

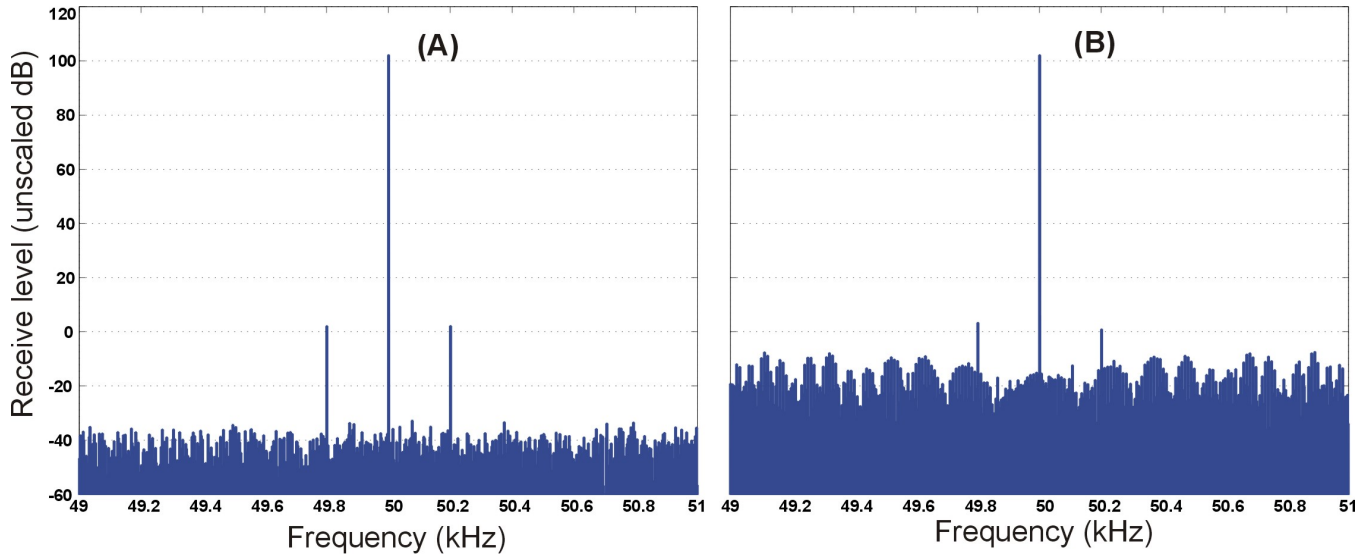

Figure 3: Spectra of Bit Coded Carrier Signals with 200 Hz Modulations. 16 Bit Coding (A) and 12 Bit Coding (B)

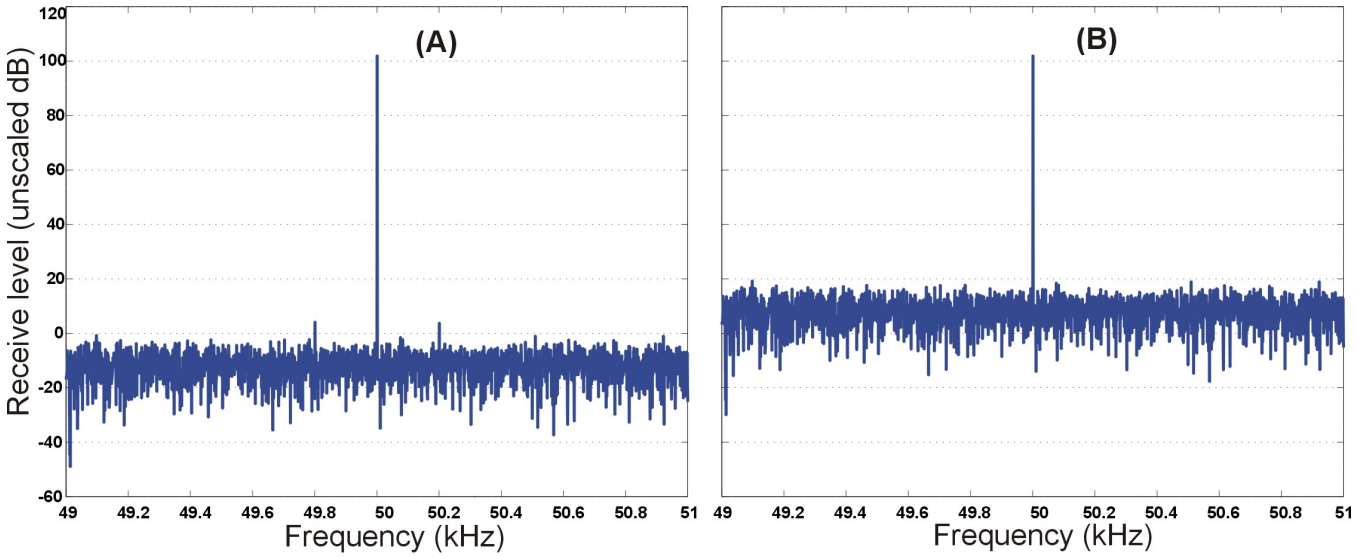

Figure 4: Spectra of Carrier Signals with 200 Hz Modulations Sampled with Clock Jitter. 5 nS Peak Random Timing Jitter (A) and 50 nS Peak Random Timing Jitter (B)

Three analog schemes were considered for the demodulation of the ultrasound signal. These involve phase-locked-loop (PLL) circuits, passive mixers, and active multipliers. The PLL was the simplest of these to implement, since several manufacturers produce integrated circuit PLLs that can operate at 50 kHz. The advantage of a PLL is that it contains an internal voltage controlled oscillator that tracks the phase of the carrier signal. The constant phase terms are thereby eliminated from expression 3, and the displacement can be deduced from the output of a single mix of the carrier with the output of the voltage controlled oscillator. Unfortunately the source of this simplicity is also a noise source similar to the clock jitter problem encountered with the digitizer. Here the VCO must be spectrally pure so that the mixer output is not contaminated by the jitter of its output signal. Single chip PLLs were not adequate to meet the signal-to-noise requirement of the ultrasound vibrometer or even to achieve the performance potential of the digitizing scheme already tested. Voltage controlled oscillators with sufficient spectral purity to construct a PLL that might achieve the desired goals were available. Because of the uncertain potential and high cost of these, the PLL demodulation scheme was not pursued. Analog mixing was

investigated with passive mixers and several types of active multipliers available as integrated circuits. Fortunately the best performance and the lowest cost among the available options was found to be the AD534 four quadrant multiplier available from Analog Devices. With these, two multiplier stages with low pass filters were constructed on a breadboard to provide the analog outputs represented by equations 3 and 5. Prepackaged high-pass and low-pass filters (Kron Hite 734) were then used to separate the outputs of these stages into the four AC and DC terms represented in equation 5. These were then acquired on four channels of the 12-bit digitizer previously described, the problems of clock jitter and bit coding having been obviated by the analog manipulations. The demodulation scheme, as it was implemented experimentally, is shown in figure 5. Bench top testing revealed a noise floor on the order of 1 nm using this demodulation scheme with the ultrasonic vibrometer operating at 50 kHz. This is equivalent to the performance of the radar sensor, although the shorter wavelength of the ultrasound (7mm vs. 38mm) would indicate that a 12-dB improvement was possible if all other factors were equal. The dominant source of noise in the ultrasonic vibrometer is not currently known, and further improvements in performance may be achieved in the ongoing work on its development and testing.

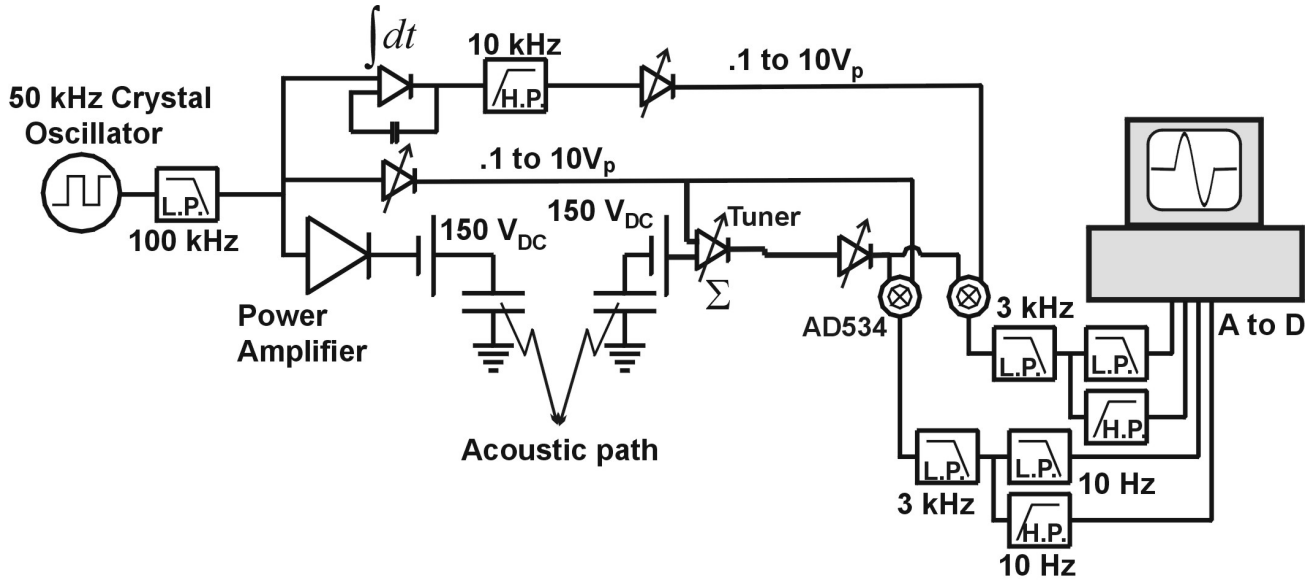

Figure 5: Prototype Ultrasonic Vibrometer Configuration

3. ULTRASONIC TRANSDUCERS

Direct scaling of the radar wavelength to an air-acoustic signal would yield an operating frequency of 9 kHz. This is within the audible range for most people and is quite annoying for many. Transducers resonant at 50 kHz are produced by several manufacturers and are available at relatively low cost. The shorter wavelengths associated with higher frequencies eased the requirements on the demodulation needed to match the signal-to-noise performance of the radar sensor. Other transducers, designed to operate in the 20 to 30-kHz range, are also commonly available. These will be tested in future realizations of the ultrasonic vibrometer in order to reduce sensitivity of the received signal to surface roughness and improve penetration of ground cover. Both capacitive and piezoelectric 50 kHz transducers were tested for the vibrometer and show similar transmitting and receiving characteristics. The capacitive transducers were selected for the first prototype vibrometer because of their smaller diameter (4cm) and, therefore, smaller beam width. These transducers operated essentially as piston sources, and they were positioned such that the soil surface was in the range of their natural focusing in order to minimize the spot size. Although comparable to the radar sensor's spot size, this was far from the diffraction limit. Focused transducers, focussing reflectors and diffracting lenses will be explored in future work on the ultrasonic vibrometer in order to reduce the spot size relative to the acoustic wavelength. Focusing with refracting lenses is problematic for ultrasound in air since solids, from which a lens might be easily fabricated, have a much higher compressional wave speed and density than air. Virtually all of the signal incident upon them would therefore be

reflected rather than refracted at the lens boundaries. Gas-filled lenses are a possibility for focusing [7], although there is very little in the available literature about the design and fabrication of these.

The prototype ultrasonic vibrometer is shown in figure 6. Here both the transmitting and receiving sensors are Polaroid electrostatic ranging transducers with 57-dB (re 20 μPa/V at 1m) transmitting voltage response at 50 kHz and –45 dB (re 1 V/Pa) receiving sensitivity. The transducers require a 150 V DC bias voltage in order to operate. This was achieved with stacks of 16 nine-volt radio batteries for each transducer. The capacitance of the transducer is quite low, 400 pf, and the cables (~7.5 m of RG58C coaxial cable) therefore reduced the effective receiving sensitivity by about 6 dB [8]. This will be corrected with a charge amplifier in future realizations of the vibrometer. The cross talk between transmitter and receiver was about 26 dB below the level of a signal reflected from a hard flat surface. The cross talk was primarily electromagnetic rather than acoustic in nature and nearly in phase with the driving signal. A differential amplifier, which is depicted in figure 5, reduced the cross talk signal by 16 dB, and the remaining signal was found to be in quadrature with the drive, indicating that further improvements would require phase shifting of the drive signal prior to the summation. The relatively weak direct coupling of the drive signal into the received signal was a benefit of the bistatic configuration. A similar level of decoupling has been achieved in the monostatic radar sensor by employing a circulator and a stub tuner in the high frequency electronics. Neither of these devices has an obvious analog for acoustic waves.

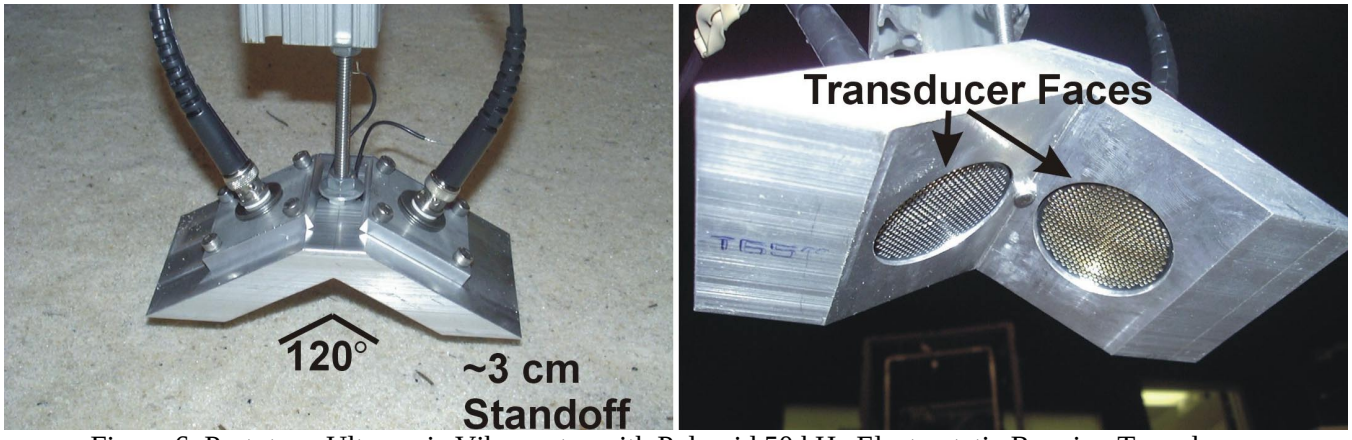

Figure 6: Prototype Ultrasonic Vibrometer with Polaroid 50 kHz Electrostatic Ranging Transducers

4. EXPERIMENTAL TESTING

The surface reflectivity of the soil surrogate in the experimental model was studied to determine both the tuning requirements and the dynamic range requirements for the ultrasonic vibrometer. The results of this study are depicted in figure 7. Here the power of the received signal is plotted on a color scale for a scan of the vibrometer over a 0.8m by 1.2m area on the surface of the soil. The received power is essentially the denominator in equation 5 and can cause the result of the computation depicted there to blow up when it becomes very small. Reflected power can therefore dictate the dynamic range of the data acquisition system. Also, as the received signal drops close to the level to which the cross talk has been tuned, the signal is diluted with the unmodulated cross talk. This causes a loss of the vibrometer calibration and gives erroneous results for the surface displacement. It can be seen in figure 7 that there are several small regions to the left center and upper left of the figure and a narrow band across the bottom where the reflected power drops sharply. Whether this is due primarily to surface roughness, absorption, or incidence angle is not known and is a subject of ongoing investigation.

The vibrometer was scanned over the same area depicted in figure 7 while a shaker source to the left of the region was driven in the 50 Hz to 2 kHz frequency range. A TS-50 plastic antipersonnel mine was buried in the center of the region with its trigger 1 cm below the soil surface. The response of this system to a 450 Hz centered pulse in the form of the first derivative of a Gaussian was reconstructed from the measured displacements. This is depicted

at three different time instants in figure 8. Here the color scale indicates the magnitude of the surface displacement from its equilibrium state. The incident wave can be seen at the first instant to be composed of a small-amplitude fast-moving wave front and a larger slower wave front. These have been determined in other measurements to be the leaky pseudo Rayleigh wave and the Rayleigh surface wave respectively. In the second instant, the surface wave can be seen to be interacting with the buried mine and to be amplified over the mine's location. In the third instant, both wave fronts have passed the mine and the motion of the mine persists because a structural resonance of the mine soil system has been excited. These results are consistent with previously reported measurements in this experimental model [2] and with numerical models [9].

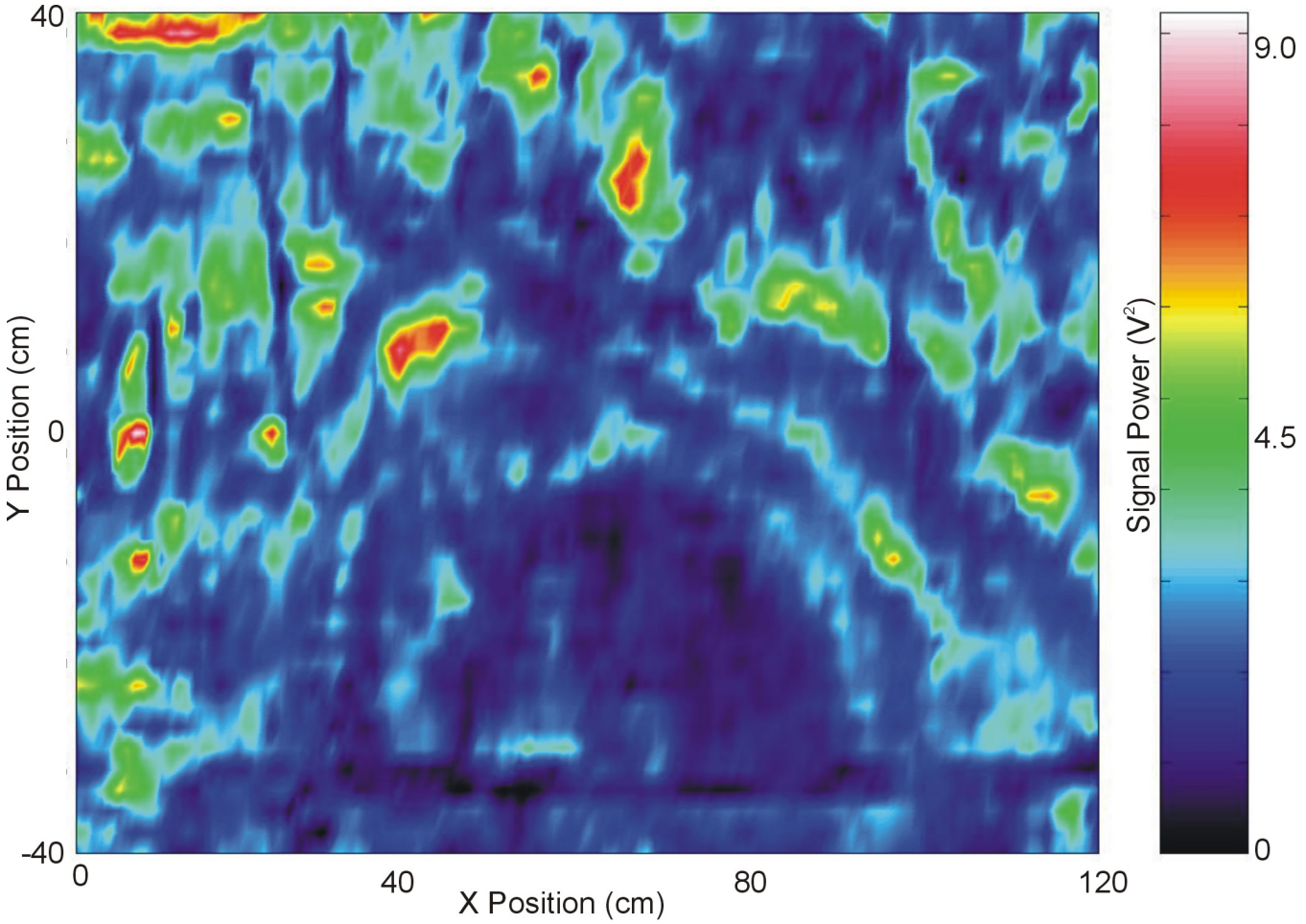

Figure 7: Ultrasonic Signal Power Reflected from the Surface of the Experimental Model in a 2-D Scan

The data depicted in figure 8 can be used to construct an image of the minefield. The procedure by which this is done has been outlined in a previous paper [10]. The procedure involves filtering in time and space to remove waves traveling away from the source, windowing the remainder in time, and plotting the RMS value within that window for each point on the measurement surface. An image that was formed in this way from the ultrasonic vibrometer data is shown in figure 9. This is similar to images formed using radar vibrometer data taken with the same model configuration. The major difference between these images is that the image in figure 9 contains an inordinate amount of clutter. This corresponds to areas where the power dropped out of the signal reflected from the surface as depicted in figure 7. Thus the clutter, although it is problematic, does not constitute a failure of the sensor concept as much as of the specific configuration used and may be fixed by better tuning, lower operating frequency, steeper incidence angle, or some combination of these.

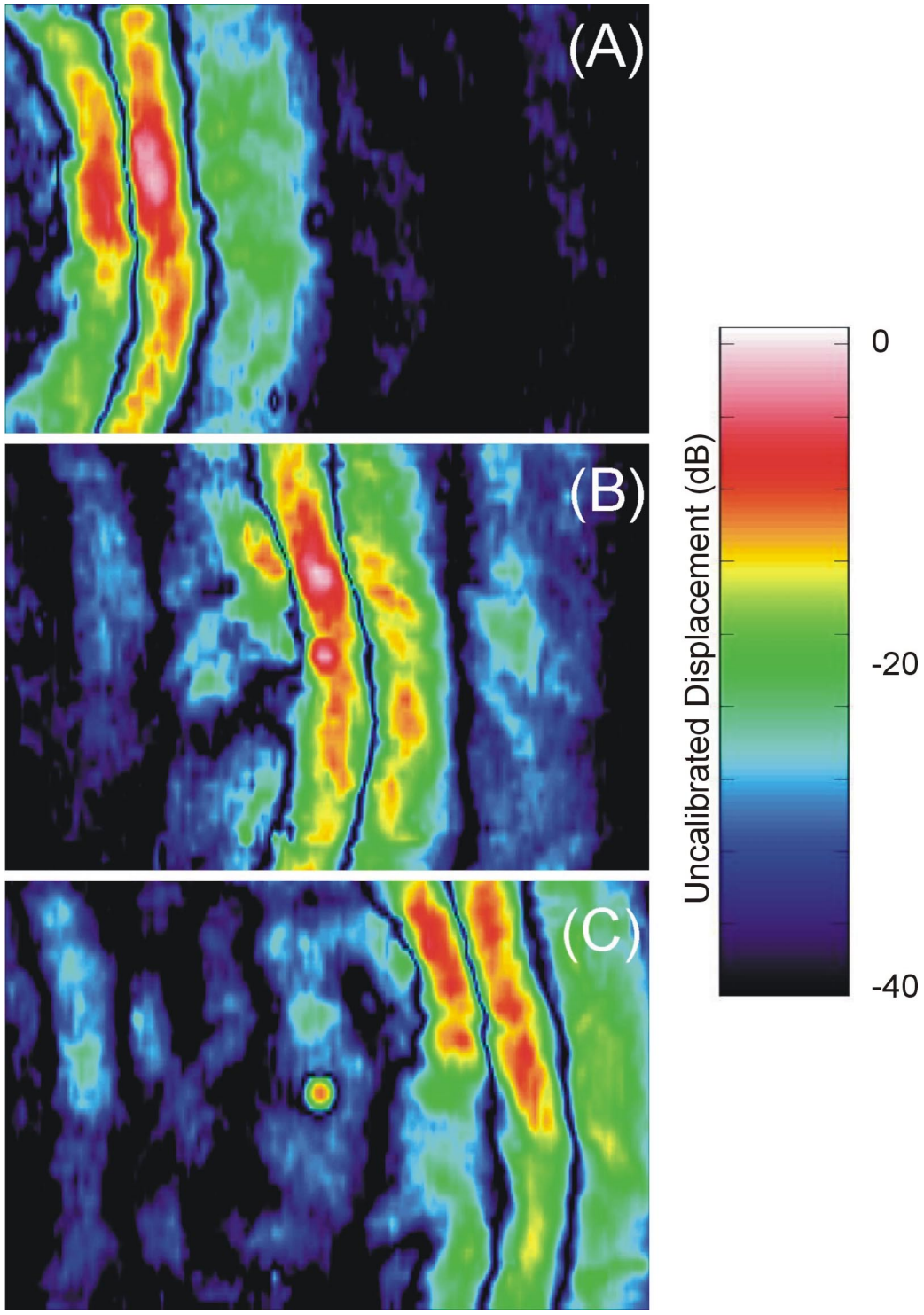

Figure 8: Absolute Displacements Measured on the Surface of the Experimental Model at 3 Instants in Time.
(A) When the leading edge of the surface wave front reaches a buried AP mine,
(B) When the main peak of the signal has reached the mine and
(C) After the wave has passed the mine.
The Scan Area is 120 cm (horizontal) by 80 cm (vertical).

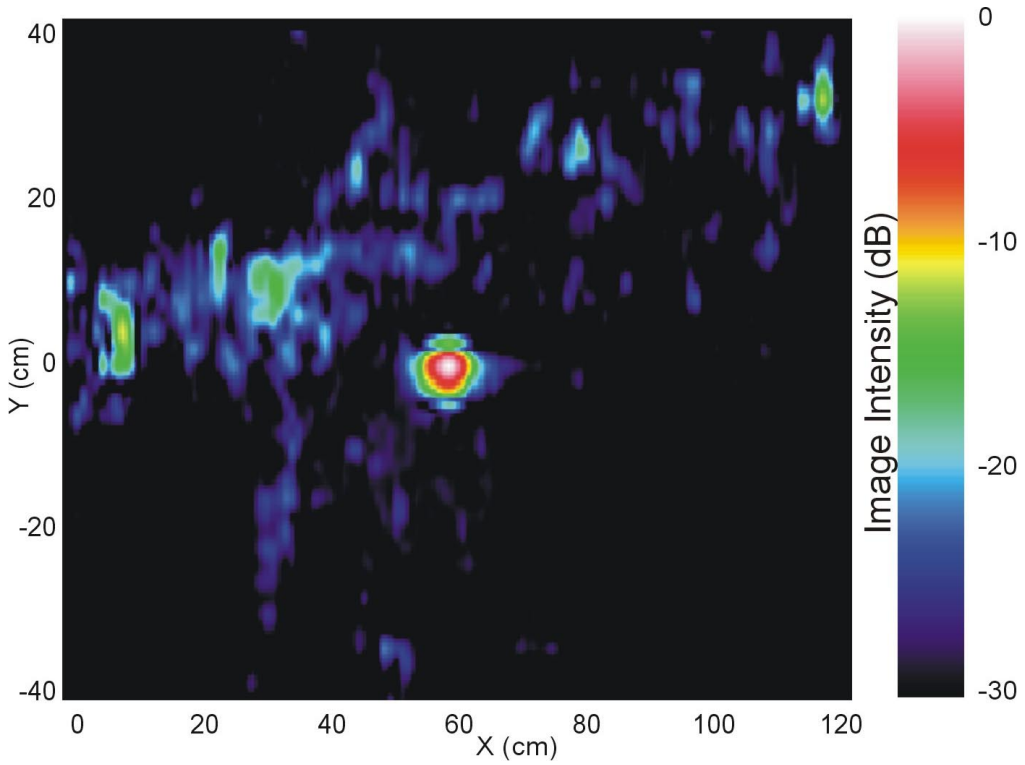

Figure 9: Image Formed of a TS-50 AP Mine Using Ultrasonic Vibrometer Data

5. CONCLUSIONS

An ultrasonic vibrometer has been constructed that mimics the performance of a previously reported radar vibrometer both in bench top tests and in a seismic mine detection. The optimal configuration of this sensor appears to be very similar to the configuration chosen for the radar sensor. Individual sensor component choices were modified to suit the much lower operating frequency corresponding to ultrasound. Although the performance of the sensor is good, several areas of improvement have been identified that will be the focus of ongoing investigations. The short-term goals of these investigations will be to optimize the design of the ultrasound vibrometer so that a comparison of it with the more-developed radar sensor can be made.

6. ACKNOWLEDGEMENTS

This work is supported in part by the Army Research Office under the OSD MURI program contract number DAAH04-96-0448 and in part by the Office of Naval Research under contract number N00014-01-1-0743.

7. REFERENCES

1. Scott, W.R., Jr., Schröder, C., and Martin, J.S., “An Acousto-Electromagnetic Sensor for Locating Land Mines,” Proceedings of the SPIE, vol. 3392, *Detection and Remediation Technologies for Mines and Minelike Targets III*, Orlando, FL, April 1998, pp. 176-186.

2. Scott, W. R., Jr., J. Martin, and G. Larson, “Experimental Model for a Seismic Landmine Detection System,” *IEEE Transactions on Geoscience and Remote Sensing*, vol. 39, no. 6, June 2001, pp. 1155-1164 .

3. “Feasibility of Acoustic Landmine Detection: Final Technical Report,” *BBN Technical Report No. 7677*, May 1992.

4. Codron, Fabien, “Detection of surface waves in the ground using an acoustic method”, *Master’s Thesis in Mechanical Engineering*, Georgia Institute of Technology, July 2000.

5. Cox, M. and Rogers, P.H., “Automated Noninvasive Motion Measurement of Auditory Organs in Fish Using Ultrasound ”, *Journal of Vibration, Stress, and Reliability in Design*, Vol. 109, January 1987, pp. 55-59.

6. Rogers, P.H. and Cox, M., “Noninvasive Vibration Measurement System”, *US Patent 4,819,649*, April 11, 1989.

7. Bobber, Robert J., “Underwater Electroacoustic Measurements”, Los Altos: Peninsula Publishing, 1988, pp. 19 and 136-7.

8. Kendall, James M., “Acoustic Lens is Gas-Filled”, *NASA Tech Briefs*, vol.5 no.3, fall 1980 pp. 345-46.

9. Schröder, C.T. and Scott W.R. Jr., “A Finite-Difference Model to Study the Elastic-Wave Interactions with Buried Land Mines”, *IEEE Transactions on Geoscience and Remote Sensing*, vol. 38, no. 6, July 2000, pp. 1505-1512 .

10. Behboodian, A., Scott, W.R., Jr. and McClellan, J.H., "Signal Processing of Elastic Surface Waves for Localizing Buried Land Mines," *Proceedings of the 33rd Assilomar Conference on Signals, Systems, and Computers*, Assilomar, CA, October 1999.